*minerals*

MDPI

*Article*

# Morphology, Mineralogy, and Chemistry of Ocherous Precipitate Aggregates Downstream of an Abandoned Mine Site

**Mitsuo Manaka**

Geological Survey of Japan, National Institute of Advanced Industrial Science and Technology (AIST), 1-1-1 Higashi, Tsukuba, Ibaraki 305-8567, Japan; mitsuo.manaka@aist.go.jp

**Abstract:** Mineral precipitates forming downstream of abandoned and/or uncontrolled mine sites generally act as scavengers for heavy metals, such as As and Sb, leaking from the sites. This study reports the morphology of ocherous precipitate aggregates downstream of Ayuta, an abandoned antimony mine site in Tochigi Prefecture, Japan, because its morphology differs significantly from those reported previously. The morphology of this aggregate consists of stacked, small terraces enclosed by numerous connected rimstone dams, although on a smaller scale compared to typical terrace landscapes. The rimstone pools contained ocherous spheroids precipitates at the bottom. Additionally, stream water and ocherous aggregates collected from the site were investigated for mineralogy and chemistry. As (0.07–0.17 μg/L) and Sb (0.02 μg/L) levels in the stream water were determined, and the distributions of As and Sb in the mineral phases of the precipitate were estimated using a sequential extraction procedure. The investigations revealed that As was adsorbed by iron-bearing ocherous precipitate aggregates, especially ferrihydrite that formed on the stream bank at concentrations, comparable to those reported by other studies (85 mg/kg). This adsorption contributed to the natural attenuation of As in the stream. Sb in the aggregate consisted of ultra-fine silt and clay-size particles of stibnite ore transported from the surrounding area and/or secondary minerals transported by groundwater and surface water.

**Keywords:** antimony; arsenic; ferrihydrite; morphology; precipitate aggregate

check for updates

**Citation:** Manaka, M. Morphology, Mineralogy, and Chemistry of Ocherous Precipitate Aggregates Downstream of an Abandoned Mine Site. *Minerals* **2021**, *11*, 32. https://doi.org/10.3390/min11010032

Received: 9 November 2020
Accepted: 25 December 2020
Published: 29 December 2020

**Publisher's Note:** MDPI stays neutral with regard to jurisdictional claims in published maps and institutional affiliations.

**Copyright:** © 2020 by the author. Licensee MDPI, Basel, Switzerland. This article is an open access article distributed under the terms and conditions of the Creative Commons Attribution (CC BY) license (https://creativecommons.org/licenses/by/4.0/).

## 1. Introduction

Precipitates formed by the dissolution and oxidation of iron and aluminum-containing minerals often occur downstream of abandoned and/or uncontrolled mine sites. Precipitates occur on river sediments [1–4], below and/or on the sides of the dam water outflow [5–7], on riverbanks [8], and in cemented layers, such as hardpans [9]. The precipitates effectively adsorb heavy metal ions, such as As and Sb, and inhibit the outflow of these ions downstream. For example, As concentration was found to be reduced to background levels by sorption onto authigenic schwertmannite while migrating from the drainage of an abandoned As mine in Nishinomaki, Japan, into a nearby river [6]. In a similar manner, Sb concentration was also found to be reduced to background levels [7]. Such natural attenuation can be helpful for removing heavy metal contaminants from the environment. Thus, numerous studies have focused on the adsorption of these ions by precipitates based on experimental results on natural and synthetic materials; however, the natural attenuation properties of iron- and/or aluminum-bearing materials are not well understood in riverbanks [8].

Ratié [8] proposed that the riverbank may act as a "biogeochemical filter" between soils and streams and could be a major mechanism for the trapping and flux regulation of heavy metal ions. Most riverbanks also possess a reactive redox interface. Ferrous iron is released in groundwater precipitates as ferric iron, in response to the diffusion of $O_2$ into the riverbank, along with adsorbing and/or capturing heavy metal ions. Thus, the iron-bearing precipitates have a potential impact on natural attenuation for heavy metals. The

existence of iron-bearing precipitates in riverbanks cannot be ignored when evaluating the transport of heavy metal ions downstream of abandoned and/or uncontrolled mine sites.

This study focused on the precipitates along the bank of a small stream in the remains of the Ayuta Mine, Tochigi Prefecture, Japan. The presence of stibnite–quartz veins suggests the Ayuta Mine once produced antimony, although details are scarce because very few records exist [10,11]. The Metal Mining Agency of Japan [10] indicates that there are many hydrothermal quartz–stibnite veins in this area formed within the Yamizo Group of the Jurassic accretionary complex that is mainly composed of sandstone, shale, and chert [11].

Precipitates protect stream banks by covering them and preventing contact with the environment. However, the degree of protection varies with the morphology of precipitates related to ambient conditions such as concentration, composition, and flow rate of the generating solutions, as well as temperature, time, and space available for precipitation [12,13]. The morphology of precipitates often reflects changing conditions during formation. Precipitate covers can limit the outflow of water from stream banks, including heavy metal ions, because precipitates generally have a lower porosity than the other materials composing stream banks. Differences in morphology may cause a difference in the limitation of outflow. In general, precipitates form as flowstones on dams [5–7], and, as opined by Ratié [8], precipitates may also form as flowstones on stream banks. However, to our knowledge, there are few reports on their morphologies as a whole, except for areas around caves and hot springs. The aim of this study was to investigate the morphological associations of precipitates on stream banks and the natural attenuation of heavy metal ions, such as As and Sb, downstream of abandoned mine sites. This study reports the discovery of an aggregate of ocherous precipitates on a stream bank near the Ayuta Mine site, with a unique morphology, and discusses its features, along with the mineralogy and chemistry.

The aggregate consisted mainly of precipitates in the stream in the remains of Ayuta Mine, Japan. Its overall morphology was segmented in a manner similar to that of a wasp nest, and the surface and internal structures of the aggregate were observed by photography and X-ray computed tomography. The mineral phases of the aggregate were determined by combining X-ray powder diffractometry (XRD) and the sequential extraction procedure, and the chemical composition of the aggregate was analyzed using inductively coupled plasma-mass spectrometry. In addition, the distribution of As and Sb in the aggregate was investigated, to confirm the natural attenuation of these metals in the stream.

## 2. Materials and Methods

### *2.1. Site Description*

Investigations were performed at the remains of the Ayuta Mine, located in the southeast region of Tochigi Prefecture in Japan (Figure 1). This mine is located approximately 3.5 km south–southwest of the Motegi Mine [10]. According to Ishihara [14], the Motegi Mine had a record of 297 tons of Sb ore (16.9% Sb) from the stibnite–quartz vein up to a strike length of 100 m. However, details of the Ayuta Mine are unknown, due to very few existing records, except for the knowledge that Sb ore was once mined from this location. A survey of the remains of Ayuta Mine could not find any adits or shafts. Thus, other fields near the Ayuta Mine were investigated, which led to the discovery of mine wastes, including Sb ore, which were sampled. This paper describes the mineralogy of the samples collected from mine waste, based on the observation of polished thin sections. The ores included stibnite, and the filling mineral included quartz. Waste rocks included pyrite, goethite, and quartz.

There are existing streams in the remains of Ayuta Mine (Figure 1). The stream water flows from site 1 to site 8 and enters a tributary to the Ayuta River. Because site 2 had an ocherous aggregate, these measurement locations were selected to investigate the natural attenuation of dissolved heavy metals, such as As and Sb. At site 2, the infiltrated waters from the north side flow out from the stream bank as seepage water. The stream beds are covered with ocherous matters around sites 2 to 3.

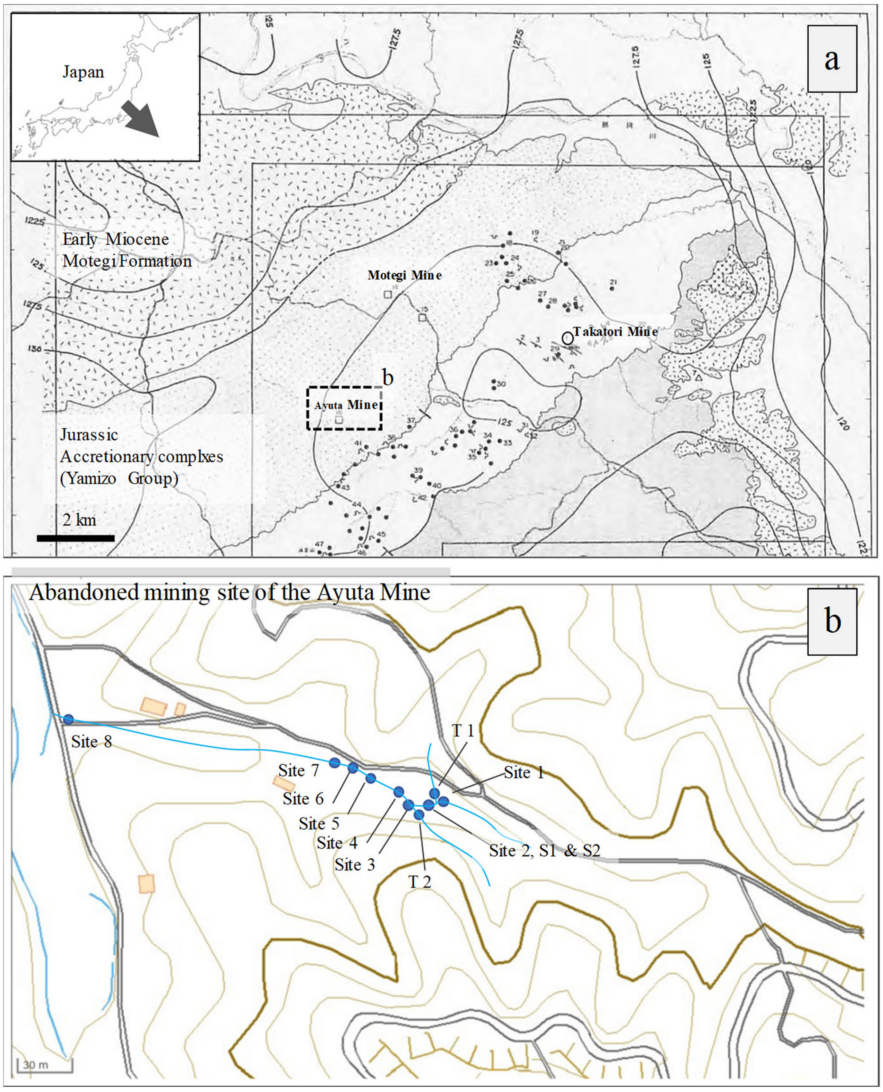



**Figure 1.** Geology and location of the Ayuta Mine, Tochigi Prefecture, Japan. (**a**) Geologic map. Geological data were compiled from the Metal Mining Agency of Japan [10] and Yoshioka et al. [11]. (**b**) Location map of the "b" position marked in (**a**). The positions of sample sites from 1 to 8 along the stream are plotted on the topographic map.

### *2.2. Analysis of Stream Water*

Stream and seepage water samples were collected at 12 sites (Figure 1). Stream water was collected from sites 2–7 in February 2007 and from sites 1–8 in December 2019. However, the discharges were not measured, although concentration levels were expected to depend on discharges. Two seepage water samples (S1 and S2) were collected, using a suction-cup (DIK-8393, Daiki Rika Kogyo, Saitama, Japan), from a stream bank behind the aggregate at site 2. In addition, tributary stream water was collected at T1 and T2. Each water sample was filtered through a 0.2 µm membrane and then divided into two portions, which were stored separately in acid-washed 50 mL polyethylene bottles. One portion of each sample was acidified with $HNO_3$ (trace analysis grade) to make an approximately 0.11 mol/L (M), or 0.35 M, $HNO_3$ solution for inductively coupled plasma-mass spectrometry (ICP-MS), while the other portion was left unacidified for analysis by ion chromatography (IC). Moreover, IC analysis was performed immediately after the samples arrived at our laboratory.

Onsite, the pH, temperature, and electric conductivity (EC) were measured with a pH meter (GST-2729C, DKK-TOA, Tokyo, Japan) and a conductivity meter (CM-21P, DKK-

TOA). The pH electrode was calibrated with standard buffer solutions (pH 4.01 and 6.86) before measuring the stream water samples. The error of the pH meter is <0.02 pH unit. The EC meter was tested using deionized distilled water and 0.1 M KCl.

Water sampled in February 2007 was analyzed by ICP-MS at Activation Laboratories (Ancaster, ON, Canada), and anion analysis was performed by ion chromatography (Shimadzu, Kyoto, Japan) at our laboratory. Analysis of duplicates for Ca and Al indicated a precision higher than 5%, while other elements indicated a precision higher than 2%. Water sampled in December 2019 was analyzed by ICP-MS (Agilent Technologies, Tokyo, Japan), and anion and cation (Na, K, Mg, and Ca) analysis was performed by ion chromatography (Thermo Scientific Dionex, Sunnyvale, CA, USA) at our laboratory. Calibration of the ICP-MS and IC for elemental concentrations was conducted using commercial aqueous standards of various elements. Analysis of duplicates for Sb indicated a precision better than 5%, while other elements indicated a precision better than 3%.

### *2.3. Analysis of Solid Phases*

At site 2, there was an aggregate composed of ocherous materials, with an appearance similar to wasp nests, which was attached to the stream bank of the north side (Figure 2). The length, width, and depth of the ocherous aggregate were approximately 30 cm, 20 cm, and 7 cm, respectively (Figure 2a,b). The ocherous aggregate samples were collected in March 2007 and December 2019. For the first collection, most of the ocherous aggregates were sampled (Figure 2c). The aggregate was air-dried at our laboratory. Before each mineral identification and chemical analysis experiment, the air-dried samples were crushed by hand, sieved through a 2-mm screen, and thoroughly mixed prior to analysis.

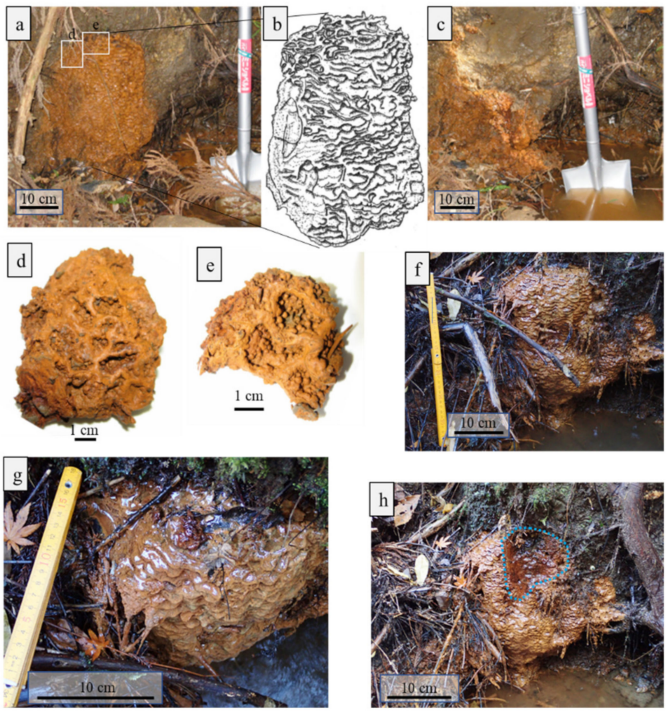



**Figure 2.** Photographs and a sketch of the ocherous aggregate at site 2. (**a**) Aggregate attached to the stream bank. (**b**) Sketch of the aggregate. (**c**) The stream bank after the aggregate was sampled in March 2007. (**d**,**e**) Enlarged photos of air-dried pieces from the "d" and "e" positions marked in (**a**), respectively. Dried rimstone pools have ocherous spheroids. (**f**) Side view and (**g**) top view photos of aggregate recovered in December 2019. (**h**) Parts (green dotted enclosed line) of the top of the aggregate were sampled in December 2019.

Part of the air-dried aggregate was powdered using a fully automatic pulverizer (HP-MS, Herzog, Germany). The powdered aggregate was analyzed with an X-ray powder diffractometer (RINT 2500V, Rigaku, Tokyo, Japan) at GSJ-Lab, AIST, using monochromatic CuKα radiation, operated at 40 kV and 100 mA. The step size was 0.02°, and the scan speed was 1 °/min. A no-reflection Si-plate sample holder was used to minimize the scattering from the holder. Clay identification and procedures using air drying and acid treatments were based on those reported by Moore and Reynolds [15].

The analysis of the sulfur content was performed on approximately 5 mg of each air-dried powder sample, using a Carlo Erba Elemental Analyzer at Tohoku University, Japan. Although the detection limit for sulfur was 0.5 g/kg, all samples collected in this study were below the detection limit for sulfur.

After the masses of the air-dried samples were determined, a sequential extraction procedure was performed to determine the distribution of As and Sb in the mineral phases of the aggregate. The extraction conditions and procedures were based on the previous reports [7,16,17]. The sequential extraction procedure consisted of two steps: (1) dissolution of poorly crystalline iron oxides by Tamm's acid oxalate (TAO) reagent [18]; and (2) dissolution of crystalline iron oxides by 6 M HCl. In addition, step 2 dissolves clay minerals, such as chlorite [15]. Following each extraction step, the samples were washed twice with 10 mL of deionized distilled water and dried overnight in a temperature-controlled box at 60 °C. After each extraction step, the suspension was centrifuged, and the supernatant and residue were immediately separated by filtration through a 0.45 μm membrane filter. The filtered solution was acidified with $HNO_3$ (trace analysis grade) for the subsequent concentration measurement of Fe, Al, Mn, As, and Sb by ICP-MS at Activation Laboratories. Analysis of the duplicates for As indicated a precision higher than 8%, while other elements indicated a precision higher than 5%. Moreover, the residuals from some of the extraction steps were analyzed using XRD [1,19].

For the second collection, the ocherous aggregate was collected at the same site in December 2019. The shape of the aggregate at the second time of the collection (Figure 2f,g) was almost restored to the shape observed at the first collection in 2007 (Figure 2a), indicating that the minimum growth rate for the shape returned it to the original size after 12 years. Immediately after the aggregate arrived at our laboratory, the aggregate was placed in a plastic box to prevent water from evaporating, and the box containing the aggregate was stored under refrigeration until an internal image could be captured by X-ray computed tomography (CT) (Supria Grande, Hitachi, Tokyo, Japan) at GSJ-Lab, AIST. The imaging settings were as follows: voltage: 120 kV; current: 150 mA; and slice thickness: 0.625 mm. The X-ray CT data obtained were processed using the open-source ImageJ software to create a cross-sectional image of the sample.

## 3. Results

### *3.1. Morphology of Ocherous Aggregate*

Figure 2 shows the characteristic morphology of the ocherous aggregate. Its morphology consists of dish-like ocherous products (~10 mm in diameter) stacked in layers and appearing as numerous connected rimstone dams (as seen in caves) that could be observed on the surface of the aggregate upon detailed inspection. The inside of dishes (rimstone pools) contained several ocherous spheroids (~1 mm in diameter) (Figure 2d,e).

The internal morphology of the ocherous aggregate can be observed from the CT images, shown in Figure 3, of slices cut parallel to the stream surface. Figure 3 shows that numerous rimstones appear to overlap, and that most of the rimstones are curved inward towards the stream side (the lower side of both photos). In addition, several spheroids were observed inside the rimstones. Although Figure 3 represents a single slice of the sample, it was confirmed that the rimstones overlap and spheroids are actually small spheres when performing three-dimensional reconstruction with consecutive CT slices.

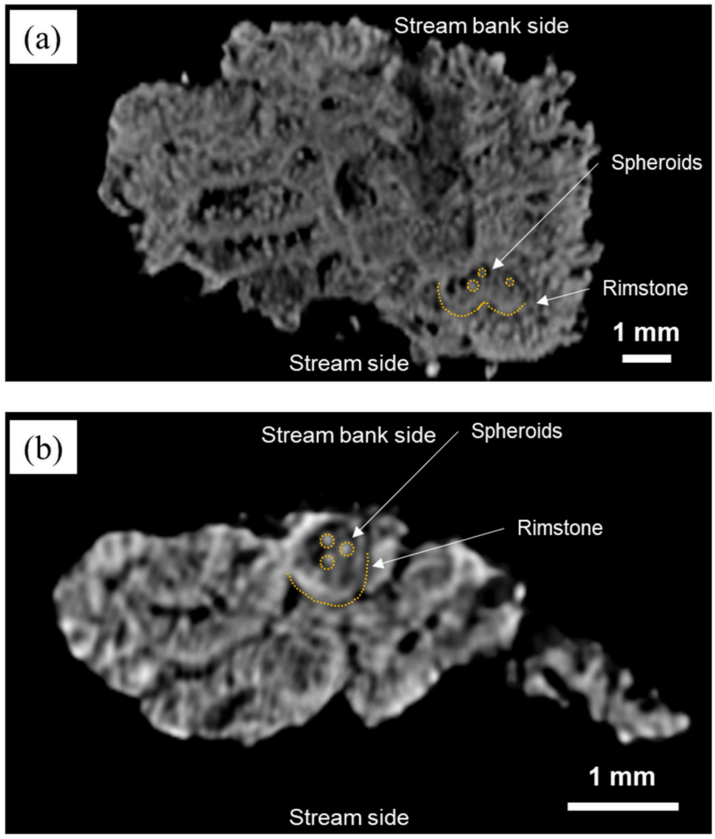



**Figure 3.** Imagery of parts of the aggregate sliced parallel to the stream surface during image processing. The upper side of both images (**a**,**b**) show the stream bank side, and the lower part of the images shows the stream side. The spheroids are gray dot-like formations in both images. As examples, a part of rimstone and spheroids is highlighted with yellow dotted lines.

### *3.2. Mineralogy of Ocherous Aggregate*

In this study, the mineral composition of the ocherous aggregate was investigated by XRD analysis. For the mineral investigation, samples of the ocherous aggregate were divided into four parts: ocherous spheroids, rimstones, rimstone basins (bottom products of the rimstone pools), and materials below the basins. As a result, there was no difference in the mineral phases for the former three. These samples contained ferrihydrite, which was identified from the XRD patterns (Figure 4a). In addition, quartz and plagioclase derived from the surrounding soils and/or rocks were detected, suggesting that the amounts of quartz and plagioclase were small due to very low intensities recorded in their XRD patterns. Thus, the mineral phases indicated that the former three were precipitates consisting primarily of ferrihydrite. In contrast, the materials below the basins consisted of crystalline mineral phases of quartz, plagioclase, illite, and layered silicate mineral with a peak of 14 Å on the XRD pattern (Figure 4b), indicating that they were derived from the surrounding soils and/or rock fragments.

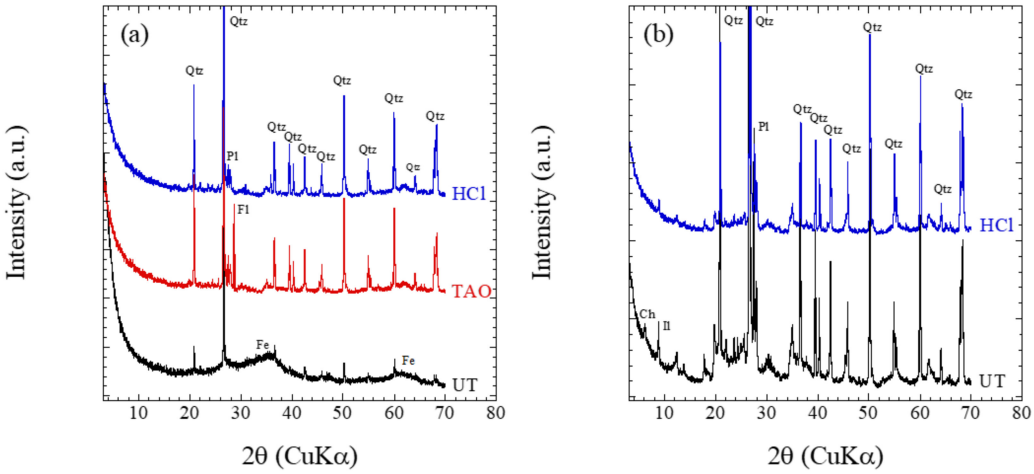



**Figure 4.** Typical XRD patterns of the aggregate before and after some sequential extractions. Abbreviations: UT: untreated samples; TAO: after Tamm's acid oxalate (TAO)-treated samples; HCl: after 6 M HCl-treated samples; Ch: chlorite; Fe: ferrihydrite; Fl: fluorite; Il: illite; Pl: plagioclase; Qtz: quartz. (**a**) Rimstone basins. Ferrihydrite has the usual peaks at about 0.26 nm and about 0.15 nm, which are broad due to weak crystallinity. The peak of fluorite appears due to disappearance of ferrihydrite by TAO treatment, but disappears with 6 M HCl treatment. Fluorite occurs as a major gangue mineral of the Takatori tungsten mine, where the Takatori mine is located approximately 6 km east of the Ayuta Mine (Figure 1) [10,11]. Thus, this area may have been mineralized by veins including fluorite in the Takatori mine. The peak strength of quartz increases with the treatments because ferrihydrite and other materials are removed in each treatment. (**b**) Materials below basins of rimstone. Materials consist of chlorite, illite, plagioclase, and quartz as crystalline minerals.

The occurrence of crystalline Fe-bearing minerals in the ocherous aggregate was then investigated by combining the extraction process and the XRD analysis. The XRD patterns of the samples before and after TAO extraction indicated that ferrihydrite as an amorphous material was present only prior to TAO extraction, quartz was present both before and after TAO extraction, and plagioclase appeared after TAO extraction (Figure 4a). Thus, the aggregate did not contain crystalline iron (oxy)hydroxides or oxides, based on the analysis result of XRD after TAO extraction, but crystalline iron (oxy)hydroxides or oxides may be present in trace amounts because XRD is less sensitive. Diffraction peaks of plagioclase appeared due to the disappearance of ferrihydrite. In contrast, the XRD patterns of materials below the basins before and after 6 M HCl extraction indicated that quartz, plagioclase, and illite were present both before and after the extraction, but the layered silicate mineral was only present prior to the extraction (Figure 4b). The layered silicate material was determined to be chlorite, as it can be dissolved by the 6 M HCl solution, which also indicated that chlorite was one of the crystalline Fe-bearing minerals in the ocherous aggregate. The above observation indicated that the ocherous aggregate consisted mainly of ferrihydrite and soil (or rock) derived from the surroundings.

### *3.3. Chemistry of Ocherous Aggregate*

The laboratory analyses confirmed that all four parts of the aggregate contained Fe, Al, Mn, As, and Sb. In general, incremental weight losses occurred when the samples were subjected to the sequential extraction procedure. The weight loss during extraction by the TAO reagent indicated the presence of amorphous materials in samples. The weight loss following the subsequent extraction by the 6 M HCl reagent indicated that some crystalline iron (oxy)hydroxides or oxides and chlorite were removed, as the amorphous materials in the samples had already been dissolved by the TAO reagent. Figure 5 shows the mass ratio of amorphous and crystalline materials and element compositions in the four parts. Ocherous spheroids, rimstone, and rimstone basins consisted of 85% or more of the amorphous materials (Figure 5a), while materials from below the basins consisted of 85% or more of other minerals such as quartz, plagioclase, and illite, based on XRD data.

The aggregate did not contain much crystalline Fe-bearing minerals, such as goethite (<5%). The main component of amorphous materials was ~35% Fe (Figure 5b), which further supports the identification of ferrihydrite by XRD analysis.

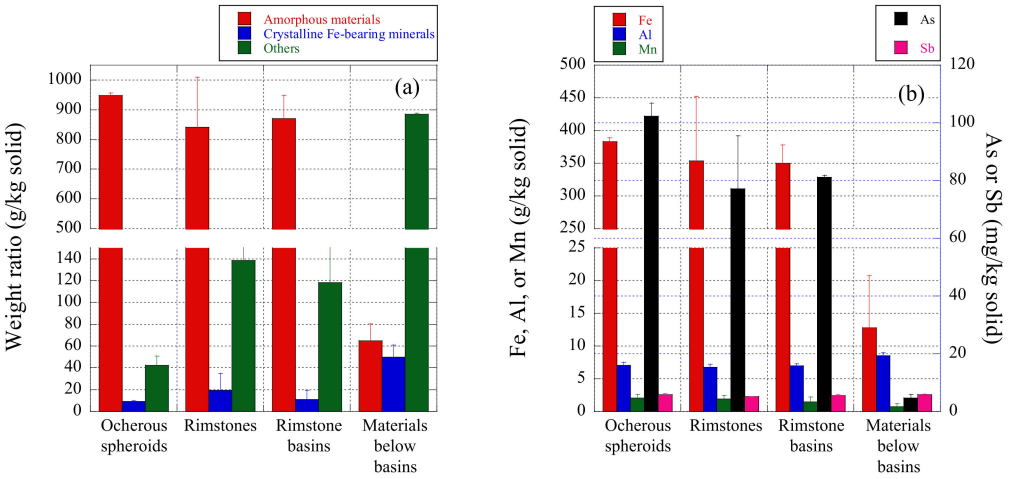



**Figure 5.** Weight ratio and element content in the four parts of the aggregate. (**a**) Weight ratios of amorphous materials, crystalline Fe-bearing minerals, and other minerals. (**b**) Fe, Al, Mn, As, and Sb contents.

### *3.4. Chemistry of Stream Water*

The concentrations of dissolved Fe, Mn, and Al from the stream decreased markedly (Figure 6), while pH, EC, and the concentrations of dissolved $Na^+$, $K^+$, $Mg^{2+}$, $Ca^{2+}$, $Cl^-$, $NO_3^-$, and $SO_4^{2-}$ were relatively constant. However, the concentration of $SO_4^{2-}$ was abnormally high at site 8 because of inputs from other unknown tributaries. Fe and Mn concentrations were highest at site 3 (233 μg/L and 29 μg/L, respectively), while Al concentrations were highest at site 2 (30.3 μg/L). The abrupt increase in dissolved Fe, Mn, and Al concentrations recorded at sites 2 and 3 can be explained by the input of seepage waters, as seepage waters contained relatively high concentrations of Fe, Mn, and Al (Figure 6). Furthermore, the addition of groundwater to the stream can occur along the streambed or the stream margin. Seepage water may carry dissolved iron as $Fe^{2+}$, which is then oxidized in the oxygen-bearing water of the stream bed/bank, or is oxidized by iron-oxidizing bacteria. Accumulation of iron precipitates may represent locations where seepage water is added to the main stream. Moreover, at site T1, where tributary stream water was collected, Fe and Al concentrations were 117 μg/L and 60 μg/L, respectively, and other solute concentrations were not significantly different from those at sites 1–3. At T2, the solute concentrations were not significantly different from those at sites 4–8.

The concentration of dissolved As from the stream decreased markedly (Figure 6). Arsenic concentrations were highest at site 3 (0.17 μg/L), which can be explained by the input of seepage water with relatively high As concentration. In contrast, the concentration of dissolved Sb was relatively constant, although seepage water has a higher Sb concentration compared to that in the stream water.

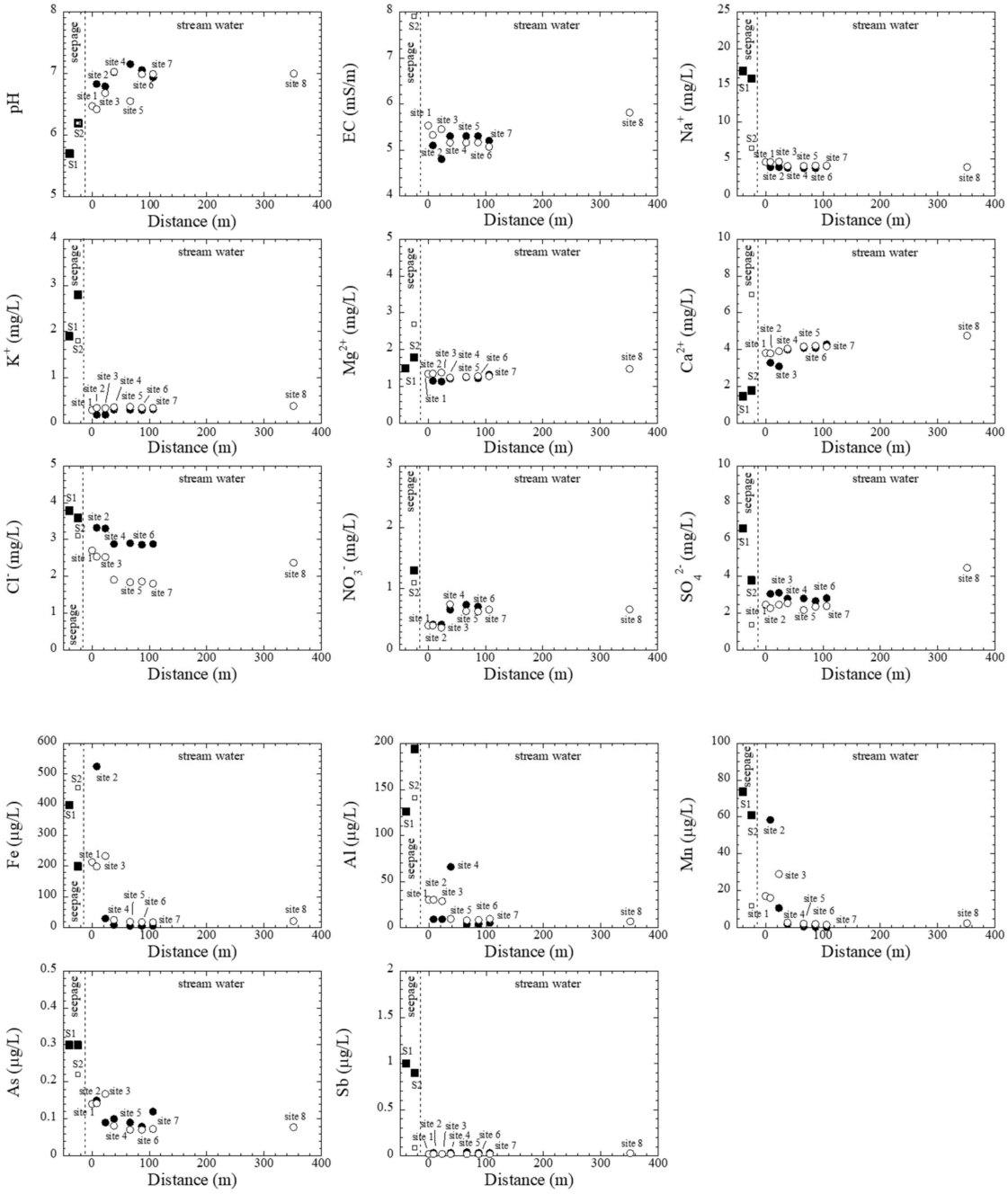



**Figure 6.** pH, electric conductivity (EC), and individual solute concentration in the samples of seepage and stream waters collected from each site. The square symbols represent seepage water and the circle symbols represent stream water. Closed symbols represent samples from March 2007 and open symbols represent symbols from December 2019.

## 4. Discussion

### *4.1. Formation of Ocherous Aggregate*

The observation of the ocherous aggregate and previous studies [12,13] indicate that the formation of aggregates can be associated with the formation location, outflow of seepage, and seepage waters highly supersaturated with respect to ferrihydrite. Thus, this study considered the formation of aggregates with respect to the above factors. The form of the aggregate was similar to those seen at rimstone systems in caves [20], although on a much smaller scale. In general, precipitates form as flowstones on stream banks, as expected from the previous studies [5–8] (Figure 7a); rimstone dams grow upward when the mineral deposition rate at the edges of the rimstone dams is faster than those at their

basins (Figure 7b). This process is expected to be caused mainly by the efficient accretion of suspended mineral particles formed in flowing water over the edges. In contrast, if there is no efficient accretion on the edges, the rimstone basin grows upward and are filled with suspended mineral particles, eventually leading to the basins having a flat formation. Based on the chemical and mineralogical analyses results in this study, the inflow from surrounding soils also contributed to the flattening of the basins (Figure 7d). After that, new rimstone dams and pools start to form on the flattening rimstone systems, and the cycle of rimstone pool formation repeats, resulting in the observed morphology (Figure 7e). During the formation of aggregates with rimstone systems, the supply of seepage water is one of the key parameters; that is, seepage water needs to flow toward and over the top surface of the growing aggregate. This condition is satisfied when the outflow position of seepage water is raised due to the barrier created by the aggregate with its low permeability, similar to the role of cemented precipitate layers [9]. In addition, the iron concentration in seepage waters needs to be supersaturated with respect to ferrihydrite, indicating that this condition was satisfied for the aggregate in this study, due to the presence of ferrihydrite. Furthermore, the occurrence of ocherous spheroids in rimstone pools was one of the significant findings in this study. Similar to the formation of cave pearls described in Jones [21], the formation of spheroids possibly occurred as suspended mineral particles adhered to the detrital nuclei, such as mineral pieces. The coated pieces were pressed against the inside of rimstone by the flow of water, newly suspended mineral particles attached to the pieces, and the grown pieces were rotated with time by the flow of water leading to the spheroids shape (Figure 7c). The reason the precipitates of ferrihydrite were divided into spheroids and rimstone dams was probably due to the fact that suspended mineral particles settle over time.

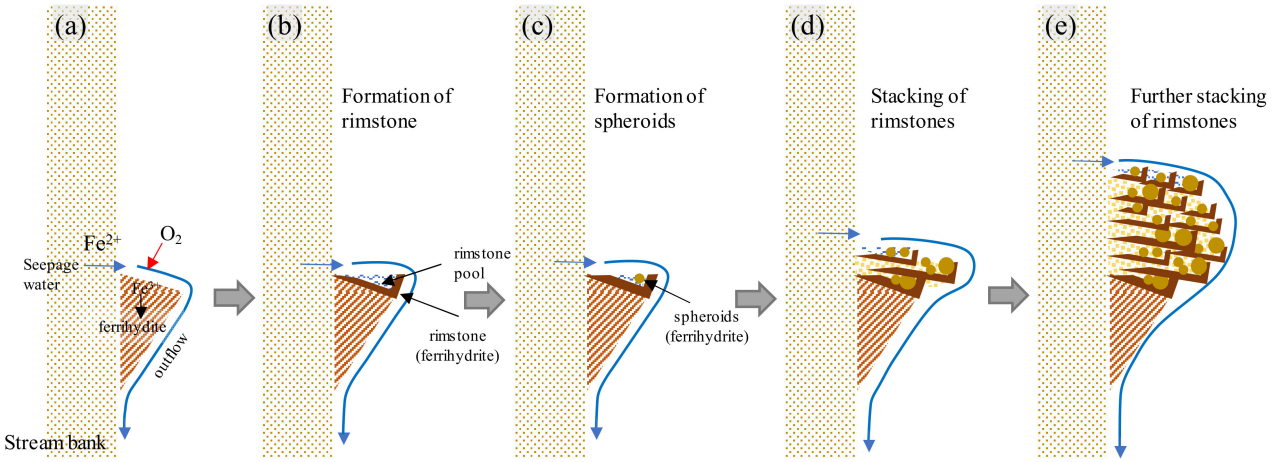



**Figure 7.** Illustration of formation of aggregate by stacking connected rimstones made of ferrihydrite. (**a**) Seepage waters flow out from the stream bank, ferrous iron in outflow water reacts with atmospheric oxygen to form ferrihydrite, which appears as flowstone on the stream bank. (**b**,**c**) Rimstones and rimstone pools are formed, along with formation of spheroids. (**d**) Rimstones are connected to each other and build up upward, along with flattening of the basins. Outflow position rises during growing rimstone systems. (**e**) Formation of connected rimstones and filling of their pools are repeated, resulting in a wasp-nest shaped morphology.

### *4.2. As and Sb Uptake by Ocherous Aggregate*

From the above mineralogical and chemical observations, the aggregate, which was attached to the stream bank, consisted mainly of ferrihydrite. Thus, considering Fe in amorphous materials, regarded as Fe in ferrihydrite, this study focused on As and Sb uptake by ferrihydrite in the aggregate. The mass of Sb extracted by the reagent was uncorrelated with the mass of Fe and Al extracted by the reagent, suggesting that ferrihydrite in the aggregate does not uptake Sb. Based on both the decrease in Sb concentration in the stream

waters and low Sb contents in the aggregate, other solid phases may be controlling Sb uptake. A possible candidate for Sb uptaker is organic matter in the stream, as inferred from Johnston [4] and Ratié [8]. In addition, the Fe-oxyhydroxysulfate mineral schwertmannite [7] and amorphous iron and manganese oxides [2] can adsorb Sb, whereas the ferrihydrite in this study area cannot. This difference may be associated with the difference in Sb adsorption sites on the surface of their materials.

The sequential extraction results showed that the mass of Fe extracted by the TAO reagent positively correlated with the mass of As extracted by the reagent (Figure 8). The slope of the regression line indicated that the apparent average concentration of As with Fe into ferrihydrite was 0.23 ± 0.02 g/kg (r = 0.976). This is related to the coexisting As concentration (approximately 0.15 μg/L) in stream water at sites 2 and 3. The apparent enrichment factor of Fe in ferrihydrite was the ratio of these two concentrations, which in this case was $1.5 \times 10^6$. The distribution coefficient ($K_d$) for As in Fe into ferrihydrite is the product of the enrichment factor and the solid–liquid ratio of the aggregate samples. The solid–liquid ratio in the aggregate sample averaged 0.83 (mL/g), based on the lost weight before and after air-drying. Thus, $K_d$ for As with Fe in ferrihydrite analyzed in this study was $1.3 \times 10^6$ (mL/g). In addition, assuming that the formula of ferrihydrite was $Fe_2O_3 \cdot 0.5H_2O$ [22], the $K_d$ value for As in ferrihydrite was $8.4 \times 10^5$ (mL/g).

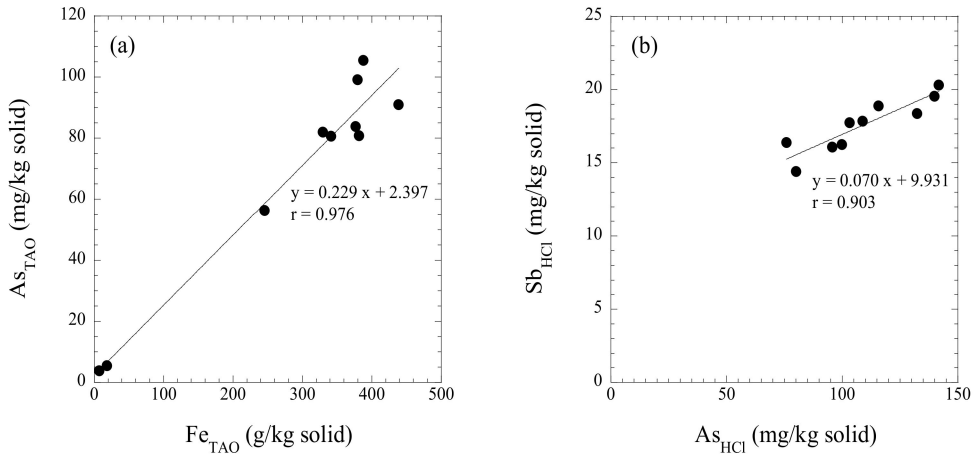



**Figure 8.** Relationship between elements extracted with each reagent. (**a**) Relationship between As and Fe contents of amorphous material as TAO soluble phase. (**b**) Relationship between As and Sb contents in 6 M HCl soluble phase. The axis label is named as follows: $Fe_{TAO}$ and $As_{TAO}$ represent the Fe and As content extracted by TAO reagent, respectively, and $Sb_{HCl}$ and $As_{HCl}$, represent the Sb and As extracted by 6 M HCl reagent, respectively.

In contrast, the mass of Fe extracted by the 6 M HCl reagent positively correlated with the mass of Al extracted by the reagent, suggesting the presence of chlorite. In addition, the mass of both As and Sb extracted by the reagent showed no correlation with the mass of Fe and Al extracted by the reagent. That is, the crystalline phase composed of Fe and Al soluble in 6 M HCl reagent was not associated with As and Sb. However, the mass of As extracted by the 6 M HCl reagent positively correlated with the Sb extracted by the reagent (Figure 8). In addition, the mass of As and Sb extracted by the reagent was equivalent to four parts in the aggregate, suggesting the occurrence of ultra-fine silt to clay-size ore particles, such as arsenic-containing Sb oxides, as an impurity that has moved from the surrounding area and/or secondary minerals, including Sb leached from Sb-bearing ores that have been transported by groundwater and surface water [2,23].

Previous laboratory studies have reported average values of $K_d$ for As in ferrihydrite, which was $3.4 \times 10^5$ (mL/g) [24,25]. All the above-reported $K_d$ values were calculated from experimental data for pH value 7. Although it is difficult to evaluate the natural values obtained, since natural conditions include many unknown parameters, it is likely

that the $K_d$ determined for As within amorphous material in this study exists in the range of the above values determined in previous studies, and this should be acknowledged. The natural $K_d$ for As should be used to predict the fate and transport of As in streams. In addition, although Pierce [24] used synthetic materials of ferrihydrite (probably powder sample) in As adsorption experiments, the $K_d$ determined for As was comparable to the amount of As adsorbed by the ocherous precipitate aggregate, thereby suggesting that the unique morphology in this study is not associated with the $K_d$ value. In other words, if the constituent mineral is the same, the $K_d$ value for a heavy metal ion presents an equivalent value. However, as this study is limited to the precipitate aggregate at this site, it is necessary to observe more precipitates on the river and/or stream banks and clarify the association with the morphology and adsorption amount for heavy metal ions.

## 5. Conclusions

The morphology of the aggregate consisting mainly of precipitates in the downstream of the abandoned site of the Ayuta Mine, Tochigi Prefecture in Japan, was shaped similar to a wasp nest, consisting of numerous stacked and connected rimstone dams, although its scale was very small compared to typical terrace landscapes. In addition, some ocherous spheroids were present in each of the rimstone pools. Rimstones, rimstone basins, and spheroids consisted of ferrihydrite. This ferrihydrite adsorbed As comparable to the amount of As in ferrihydrite reported previously, and contributed to the natural attenuation of As in this stream. In contrast, Sb in the aggregate occurred as ultra-fine silt or clay-size particles that had moved from the surrounding area and/or secondary minerals formed in transported groundwater and surface water. Natural attenuation of Sb in this stream was controlled by solid phases other than ferrihydrite.

In summary, precipitates formed downstream of an abandoned mine site can capture heavy metal ions flowing downstream from the mine site. All heavy metal ions cannot be captured by the precipitates; however, the heavy metal ions that are not captured naturally decrease while flowing downstream. Thus, it is widely accepted that precipitate aggregates do not alone contribute to the natural attenuation of heavy metal ions in the area; the uptake by precipitates and/or other solid phases in the riverbed and the dilution by the addition of stream water and groundwater also contribute to natural attenuation. In addition, although the present study was limited to the whole morphology of ocherous precipitate aggregates downstream of an abandoned mine site, it was shown that the precipitates capture heavy metal ions, regardless of their morphology. However, more observations of the internal morphology of the precipitates, along with analysis of chemical composition, is needed to clarify the association with the morphology and adsorption amount for heavy metal ions. A better understanding of the morphology, mineralogy, and chemistry of the whole and interior of precipitates will help evaluate the effectiveness of natural attenuation to remove heavy metal ions in rivers and/or streams in the vicinity of mining sites.

**Funding:** This research received no external funding.

**Data Availability Statement:** The data presented in this study are available in article.

**Acknowledgments:** The author wishes to thank Toru Shimizu for sampling and fruitful comments and discussions. The author also wishes to thank Yoshito Nakashima and Kumi Yokoi for measuring pieces of aggregate using X-ray computed tomography. The author wishes to thank Akira Ohwada, Takumi Sato, Eri Hirabayashi, and Kazuyuki Fukuda for preparing the polished thin sections.

**Conflicts of Interest:** The author declares no conflict of interest.

## References

1. McCarty, D.K.; Moore, J.N.; Marcus, W.A. Mineralogy and trace element association in an acid mine drainage iron oxide precipitate; comparison of selective extractions. *Appl. Geochem.* **1998**, *13*, 165–176. [CrossRef]
2. Filella, M.; Philippo, S.; Belzile, N.; Chen, Y.; Quentel, F. Natural attenuation processes applying to antimony: A study in the abandoned antimony mine in Goesdorf, Luxembourg. *Sci. Total Environ.* **2009**, *407*, 6205–6216. [CrossRef] [PubMed]

3. Baleeiro, A.; Fiol, S.; Otero-Fariña, A.; Antelo, J. Surface chemistry of iron oxides formed by neutralization of acidic mine waters: Removal of trace metals. *Appl. Geochem.* **2018**, *89*, 129–137. [CrossRef]
4. Johnston, S.G.; Karimian, N.; Burton, E.D. Seasonal temperature oscillations drive contrasting arsenic and antimony mobilization in a mining-impacted river system. *Water Resour. Res.* **2020**, *56*, e2020WR028196. [CrossRef]
5. Webster, J.G.; Swedlund, P.J.; Webster, K.S. Trace Metal Adsorption onto an Acid Mine Drainage Iron (III) Oxy Hydroxy Sulfate. *Environ. Sci. Technol.* **1998**, *32*, 1361–1368. [CrossRef]
6. Fukushi, K.; Sasaki, M.; Sato, T.; Yanase, N.; Amano, H.; Ikeda, H. A natural attenuation of arsenic in drainage from an abandoned arsenic mine dump. *Appl. Geochem.* **2003**, *18*, 1267–1278. [CrossRef]
7. Manaka, M.; Yanase, N.; Sato, T.; Fukushi, K. Natural attenuation of antimony in mine drainage water. *Geochem. J.* **2007**, *41*, 17–27. [CrossRef]
8. Ratié, G.; Vantelon, D.; Kalahroodi, E.L.; Bihannic, I.; Pierson-Wickmann, A.C.; Davranche, M. Iron speciation at the riverbank surface in wetland and potential impact on the mobility of trace metals. *Sci. Total Environ.* **2019**, *651*, 443–455. [CrossRef] [PubMed]
9. Elghali, A.; Benzaazoua, M.; Bussière, B.; Kennedy, C.; Parwani, R.; Graham, S. The role of hardpan formation on the reactivity of sulfidic mine tailings: A case study at Joutel mine (Québec). *Sci. Total Environ.* **2019**, *654*, 118–128. [CrossRef] [PubMed]
10. Metal Mining Agency of Japan. *Geologic Map of Kasama District, 1:25,000*; Metal Mining Agency of Japan: Tokyo, Japan, 1987. (In Japanese)
11. Yoshioka, T.; Takizawa, F.; Takahashi, M.; Miyazaki, K.; Banno, Y.; Yanagisawa, Y.; Takahashi, Y.; Kubo, K.; Seki, Y.; Komazawa, M.; et al. *Geological Map of Japan 1:200,000, Mito, Quadrangle Series 1:200,000, Mito NJ-54-24*; Geological Survey of Japan: Tsukuba, Japan, 2001; (In Japanese with English abstract).
12. Dong, G.; Morrison, G.; Jaireth, S. Quartz textures in epithermal veins, Queensland; classification, origin and implication. *Econ. Geol.* **1995**, *90*, 1841–1856. [CrossRef]
13. Sunagawa, I. *Crystals: Growth, Morphology, and Perfection*; Cambridge University Press: Cambridge, UK, 2005.
14. Ishihara, S. On the main antimony ore deposits in Japan and their genetic problems. *Shigen Chishitsu* **2012**, *62*, 151–161, (In Japanese with English abstract).
15. Moore, D.M.; Reynolds, R.C. *X-ray Diffraction and the Identification and Analysis of Clay Minerals*, 2nd ed.; Oxford University Press: Oxford, UK, 1997.
16. Schwertmann, U.; Cornell, R.M. *Iron Oxides in the Laboratory*; VCH Publishers: Weinheim, Germany, 1991.
17. Yanase, N.; Sato, T.; Isobe, H.; Sekine, K. Selective extraction procedure and its importance in a natural analogue study—Case study at the Koongarra uranium deposit. *Radioact. Waste Res.* **1996**, *2*, 121–135, (In Japanese with English abstract).
18. Tamm, O. Über die Oxalatemethode in der chemischen Bodenanalyse. *Medd. Statens Skogsförsöksanstalt.* **1932**, *27*, 1–20.
19. Kodama, H.; Kotlyar, L.S.; Ripmeester, J.A. Quantification of crystalline and non-crystalline material in ground kaolinite by X-ray powder diffraction, infrared solid-state nuclear magnetic resonance and chemical dissolution analysis. *Clays Clay Miner.* **1989**, *4*, 364–370. [CrossRef]
20. Dreybrodt, W.; Gabrovšek, F. Small-scale terraces and isolated rimstone pools on stalagmites in caves exhibit striking similarity to large-scale terrace landscapes at hot springs. *Acta Carsol.* **2009**, *38*, 19–26. [CrossRef]
21. Jones, B. Cave Pearls—The Integrated Product of Abiogenic and Biogenic Processes. *J. Sediment. Res.* **2009**, *79*, 689–710. [CrossRef]
22. Barthelmy, D. Mineralogy Database. 2014. Available online: http://www.webmineral.com (accessed on 14 May 2020).
23. Kerr, G.; Pope, J.; Trumm, D.; Craw, D. Experimental metalloid mobilisation from a New Zealand orogenic gold deposit. *Mine Water Environ.* **2015**, *34*, 404–416. [CrossRef]
24. Pierce, M.L.; Moore, C.B. Adsorption of arsenite and arsenate on amorphous iron hydroxide. *Water Res.* **1982**, *16*, 1247–1253. [CrossRef]
25. Swedlund, P.J.; Webster, J.G. Arsenic removal from geothermal bore waters: The effect of monosilicic acid. In *Water-Rock Interaction, Proceedings of the 9th International Symposium on Water-Rock Interaction, WRI-9, Taupo, New Zealand, 30 March–3 April 1998*; Arehart, G.B., Hulston, J.R., Eds.; Balkema: Rotterdam, The Netherlands, 1998; pp. 947–950.